Engineering Microbiology 3 (2023) 100106

Contents lists available at ScienceDirect

Engineering Microbiology

journal homepage: www.elsevier.com/locate/engmic

Original Research Article

Recombineering enables genome mining of novel siderophores in a non-model *Burkholderiales* strain

Xingyan Wang, Haibo Zhou, Xiangmei Ren, Hanna Chen, Lin Zhong, Xianping Bai, Xiaoying Bian*

Helmholtz International Lab for Anti-Infectives, State Key Laboratory of Microbial Technology, Shandong University–Helmholtz Institute of Biotechnology, Shandong University, Qingdao 266237, China

ARTICLE INFO

Keywords:
Burkholderiales
Recombineering
Siderophore
Genome mining
Caribactins

ABSTRACT

Iron is essential for bacterial survival, and most bacteria capture iron by producing siderophores. *Burkholderiales* bacteria produce various types of bioactive secondary metabolites, such as ornibactin and malleobactin siderophores. In this study, the genome analysis of *Burkholderiales* genomes showed a putative novel siderophore gene cluster *crb*, which is highly similar to the ornibactin and malleobactin gene clusters but does not have *pvdF*, a gene encoding a formyltransferase for N-δ-hydroxy-ornithine formylation. Establishing the bacteriophage recombinase Redγ-Red$\alpha\beta$7029 mediated genome editing system in a non-model *Burkholderiales* strain *Paraburkholderia caribensis* CICC 10960 allowed the rapid identification of the products of *crb* gene cluster, caribactins A-F (**1–6**). Caribactins contain a special amino acid residue N-δ-hydroxy-N-δ-acetylornithine (haOrn), which differs from the counterpart N-δ-hydroxy-N-δ-formylornithine (hfOrn) in ornibactin and malleobactin, owing to the absence of *pvdF*. Gene inactivation showed that the acetylation of hOrn is catalyzed by CrbK, whose homologs probably not be involved in the biosynthesis of ornibactin and malleobactin, showing possible evolutionary clues of these siderophore biosynthetic pathways from different genera. Caribactins promote biofilm production and enhance swarming and swimming abilities, suggesting that they may play crucial roles in biofilm formation. This study also revealed that recombineering has the capability to mine novel secondary metabolites from non-model *Burkholderiales* species.

1. Introduction

Iron plays an essential role in bacterial survival; for example, aerobic microbes require metal iron for reducing DNA precursors, ATP synthesis, and other processes [1,2]. However, the availability of free iron necessary for bacteria to survive in environments, such as the rhizosphere, soil, and host organisms, is limited [3]. To capture iron, bacteria have evolved various siderophores managed by the ferric-uptake regulator (Fur) [4–6]. Siderophores have various pharmaceutical applications, including reducing metal overload, diagnostics, and targeted antibiotic delivery [4]. Therefore, exploring novel siderophores and their functions is crucial.

The gram-negative bacterium *Burkholderiales* belongs to the class β-proteobacteria and lives in diverse environments, such as soil, water, and landfills, and as parasites in eukaryotic hosts [7]. These wide niches translate into various natural products, including nonribosomal peptides (NRPs), polyketides (PKs), and hybrid PKs-NRPs [8,9], which exhibit rich bioactivities, such as antibacterial, antifungal, cytotoxic, and iron-chelating properties [10,11]. *Burkholderiales* produce several types of siderophores, including ornibactins, malleobactins, pyochelin, cepabactin, and cepaciachelin, to help existence or protect themselves from toxic metals [12,13].

Burkholderiales are also an emerging source of cryptic biosynthetic gene clusters (BGCs) for novel secondary metabolites [10,14–16]. However, the absence of efficient gene editing systems for some non-model *Burkholderiales* strains limits the genomics-guided mining of cryptic BGCs in native producers [17–19]. Our group has developed several bacteriophage recombinases, Red$\alpha\beta$7029 from *Schlegelella brevitalea*, BAS from *Pseudomonas aeruginosa*, and RecET-like recombinases from *Burkholderia* spp. [20–23], which can mediate efficient recombineering for genome editing not only in the native strain but also in some other non-model *Burkholderiales* strains. These genome editing systems facilitate genome mining of cryptic BGCs in *Burkholderiales* to identify a series of novel natural products, such as, glidopeptin A, glidomides, haereomegapolitanins, burriogladiodins, and haereogladiodins [20,24–27].

In the process of mining new natural products or siderophores from *Burkholderiales* strains, the strain CICC 10960 revealed potent siderophore activity. In this study, we built a recombineering system in this strain to verify the structures and biosynthetic pathway of a class of

* Corresponding author.
E-mail address: bianxiaoying@sdu.edu.cn (X. Bian).

https://doi.org/10.1016/j.engmic.2023.100106
Received 16 May 2023; Received in revised form 30 July 2023; Accepted 31 July 2023
Available online 2 August 2023

new siderophores, caribactins A–F (**1–6**), under the guidance of genome sequencing. The caribactins promoted the production of biofilm and enhanced swarming and swimming abilities.

2. Material and methods

2.1. Bacterial acquisition and phylogenetic analysis

Burkholderia sp. CICC 10960 was purchased from the China Center of Industrial Culture Collection (CICC) and was originally isolated from the root of noni (*Morinda citrifolia*) in Sanya, Hainan, China. The Basic Local Alignment Tool was used to identify the 16S rRNA gene sequences of *Burkholderia* sp. CICC 10960, showing a high degree of similarity with *Paraburkholderia caribensis*. *Paraburkholderia caribensis* CICC 10960 and its mutant strains were cultured on M9 medium (glucose 10 g L^{-1}; K_2HPO_4 7 g L^{-1}; KH_2PO_4 2 g L^{-1}; $(NH_4)_2SO_4$ 1 g L^{-1}; sodium citrate 0.5 g L^{-1}; $MgSO_4$ 0.1 g L^{-1}) and CYMG medium (casein peptone 8 g L^{-1}; yeast extract 4 g L^{-1}; $MgCl_2{\cdot}6H_2O$ 8.06 g L^{-1}; glycerol 5 mL L^{-1}).

2.2. Fermentation, extraction, and isolation

Paraburkholderia caribensis CICC 10960 were fermented in 50 mL M9 medium in a 250 mL flask at 30 °C and 200 rpm for 3 d; next, 2% XAD-16 resin was added, followed by incubation for 1 d. The resin and bacteria were collected via centrifugation at 8000 rpm for 5 min and then extracted using MeOH (35 mL) for 3 h. The extract was then evaporated and dissolved in 1 mL MeOH. Subsequently, the extracts were analyzed using HPLC-MS and CAS assays. A total of 8.5 L of culture was prepared to purify caribactins, and the final crude extracts were subjected to vacuum liquid chromatography on a polyacrylamide gel column using MeOH and separated into several fractions. Semipreparative reverse-phase HPLC using ACN and H_2O containing 0.1% TFA as solvents A and B was used to further purify the fractions containing the target compounds under the following conditions: 0–4 min, 15% ACN; 4.1–35 min, 15–35% ACN; 35.1–45 min, 35–50% ACN; 45.1–50 min, 95% ACN; and 50.1–55 min, 5% ACN. Three compounds were obtained: **1** (9 mg), **2** (4 mg), and **3** (5 mg). Compounds were identified using HRESIMS, NMR, CD, and Marfey's analysis.

Caribactin-C_8 (**1**): white power; ^1H and ^{13}C NMR, Table S1; HRESI/MS: *m/z* 751.4199 $[M + H]^+$ (calculated for $C_{31}H_{58}N_8O_{13}$, 750.4123); $[\alpha]_D^{25}$ + 8.8 (*c* 0.08, MeOH); ECD (0.7 × 10^{-3} M in MeOH) λ_{max} ($\Delta\varepsilon$) 228 (+4.16)

Deoxycaribactin-C_8 (**2**): white power; ^1H and ^{13}C NMR, Table S2; HRESI/MS: *m/z* 735.4261 $[M + H]^+$ (calculated for $C_{31}H_{58}N_8O_{12}$, 734.4174); $[\alpha]_D^{25}$ + 13.4 (*c* 0.1, MeOH); ECD (0.68 × 10^{-3} M in MeOH) λ_{max} ($\Delta\varepsilon$) 228 (+3.53)

Caribactin-C_{10} (**3**): white power; ^1H and ^{13}C NMR, Table S3; HRESI/MS: *m/z* 779.4521 $[M + H]^+$ (calculated for $C_{33}H_{62}N_8O_{13}$, 778.4436); $[\alpha]_D^{25}$ + 3.7 (*c* 0.2, MeOH); ECD (0.64 × 10^{-3} M in MeOH) λ_{max} ($\Delta\varepsilon$) 228 (+3.09)

2.3. Marfey's analysis

Compound **1** (1 mg) was dissolved in 500 μL 57% HI. Next, the solution was heated at 105 °C for 18 h. The resulting hydrolysates of the caribactins were dried under vacuum and then re-dissolved in 200 μL ddH_2O. To derivatize the amino acids, 25 μL 1 N $NaHCO_3$ and 200 μL of a 1% Marfey's reagent solution in acetone were added and mixed. The reaction mixtures were then incubated at 40 °C for 1 h and quenched with 10 μL 2 M HCl. The amino acid standards were derivatized using a similar method [28]. To analyze L/D Ser and L/D Orn, linear gradient elution was performed from 5% to 55% ACN over 15 min at a flow rate of 0.3 mL min^{-1}. For *threo/erythro-β*-OH-D/L-Asp, the mixtures were eluted with a linear gradient from 5% to 40% ACN over 38 min at a flow rate of 0.3 mL min^{-1}. The retention times and molecular weights of caribactin-C_8 and the standard amino acids are listed in Fig. S1.

2.4. Construction of recombineering system in P. caribensis CICC 10960

Paraburkholderia caribensis CICC 10960 and its mutant strains were cultured on CYMG medium broth or agar plates at 30 °C. The mutant strains were isolated from media containing 20 μg mL^{-1} kanamycin [km], 30 μg mL^{-1} gentamicin [genta], and 30 μg mL^{-1} apramycin [apra]. Genome editing is mediated by linear and circular homologous recombination. In this study, three recombination systems, Red$\gamma\beta\alpha$, Redγ-Red$\alpha\beta$7029, and Redγ-BAS, were used [20–22]. Recombination efficiency was investigated by replacing the biosynthetic gene cluster fragment (2,228,707–2,229,924) with the apramycin resistance gene using different lengths of homologous arms (50 bp, 75 bp, 100 bp) in *P. caribensis* CICC 10960/pBBR1-Rha-Redγ-Red$\alpha\beta$7029-km, CICC 10960/pBBR1-Rha-Redγ-BAS-km, and CICC 10960/pBBR1-Rha-Red$\gamma\beta\alpha$-km.

2.5. Inactivation of crbI, crbK, and crbL, and complementary expression of crbK

The target gene was knocked out using an apramycin or gentamicin resistance gene, which was mediated by the Redγ-Red$\alpha\beta$7029 recombinant system. The resistance gene was high-fidelity amplification with *ApexHF* HS DNA polymerase from Accurate Biology Co. Ltd. (China) and flanked by homologous arms (50 bp). The templates for gentamicin resistance gene (*genta^R*) and apramycin resistance gene (*apra^R*) were plasmids R6K-lox71-genta-lox66-FleQ and RK2-apra-cm, respectively. The purified PCR products were transformed into *P. caribensis* CICC 10960/pBBR1-Rha-Redγ-Red$\alpha\beta$7029-km. Recombinants were selected on CYMG plates containing gentamicin (30 μg mL^{-1}) or apramycin (30 μg mL^{-1}). The *crbK* and chloramphenicol resistance gene (*cm^R*) were PCR amplified using the *P. caribensis* CICC 10960 genome and RK2-apra-cm as templates, respectively. A cassette containing *cm^R* and gene *crbK* was inserted into pBBR1-Rha-Redγ-Red$\alpha\beta$7029-km by using a round of Red$\alpha\beta$ recombineering. The resulting plasmid pBBR1-*crbK* was electroporated into *P. caribensis* CICC 10960 Δ*crbK* /pBBR1-Rha-Redγ-Red$\alpha\beta$7029-km. Recombinants were selected on CYMG plates containing chloramphenicol (350 μg mL^{-1}). The recombinants generated in this study are listed in Table S4. The correct recombinants were verified via colony PCR using the primers listed in Table S5.

2.6. Chrome azurol S assay

CTAB (21.9 mg) was melted in 25 mL H_2O at 35 °C, and 1.5 mL 1 mM ferric chloride (III) solution (dissolved in 10 mM HCl aqueous solution) and 7.5 mL 2 mM CAS aqueous solution were added to produce CTAB-CAS-Fe. MES (9.76 g) was dissolved in 50 mL H_2O, and the pH was regulated to 5.6 with a KOH solution. The CTAB-CAS-Fe(III) solution was mixed with MES buffer and diluted to 100 mL with H_2O to obtain an improved CAS analysis solution [29]. Next, CAS detection solution (50 μL) was added to a 96-medium microporous culture plate and mixed with 50 μL caribactins, ornibactin-C_8, or desferrioxamine B solution to obtain the final concentration range of 640 μM to 5 μM. The mixture was incubated at 37 °C for 3 h, and the resulting color of the mixture was visually observed.

2.7. Biofilm assay

Paraburkholderia caribensis CICC 10960 and *P. caribensis* mutant CICC 10960 Δ*crbI* were cultured overnight, transferred 100 μL culture to 900 μL CYMG medium, cultured at 30 °C and 950 rpm for 48 h, and rested at 30 °C for 24 h. Next, 1 mL PBS (pH 7.4) was used to wash off the suspended cells, and 1 mL crystal violet (0.1%) was used to stain the biofilm. After 15 min, the crystal violet was removed, 1 mL ddH_2O was added to wash twice, and 1 mL ethanol (95%) was added. One hundred microliters of each sample to 96-well microplate were used to measure the absorbance of OD_{600} nm using a microplate reader.

2.8. Swarming and swimming assay

For the preparation of the swarming and swimming assays, 15 mL hot CYMG-0.5% agar was poured into culture dishes and left to dry [30,31]. The overnight bacterial culture in CYMG was diluted to an OD_{600} of 0.1. Next, 3 μL of the mixture was dropped onto the center of each agar plate. The plates were incubated at 30 ˚C for 36 h.

3. Results and discussion

3.1. Genome sequence analysis of strain CICC 10960

The non-model strain CICC 10960 was originally isolated from the root of noni (*Morinda citrifolia*) in Sanya, Hainan, China, by the CICC. The crude extract showed potent siderophore activity with a positive response to chrome azurol S (CAS) (Fig. 1A). This strain was originally named *Burkholderia* sp. CICC 10960. However, the 16S rRNA sequence showed high similarity to *Paraburkholderia caribensis,* which does not belong to the *Burkholderia* genus. For further insights into this siderophore, the whole genome of *P. caribensis* CICC 10960 was sequenced using the PacBio Sequel platform. The genome consisted of three chromosomes with a total length of 8,752,342 bp and an average GC content of 62.66%. AntiSMASH analysis [32] showed 12 putative BGCs in the genome (Table S6). An NRPS BGC *crb* (GenBase Accession C_AA017426.1) on chromosome 2 shares a high degree of identity with the *orb* BGC of the siderophore ornibactin and *mba* BGC of malleobactin [33], suggesting that it is responsible for the production of siderophores, designated as caribactins. Comparative analysis of *crb* BGCs with *orb* and *mba* BGCs revealed that they possess similar genes (that is, *crbI* and *crbJ*) encoding tetramodular NRPSs CrbI (A_1-T_1, C_2-A_2-T_2-E, C_3-A_3-T_3)

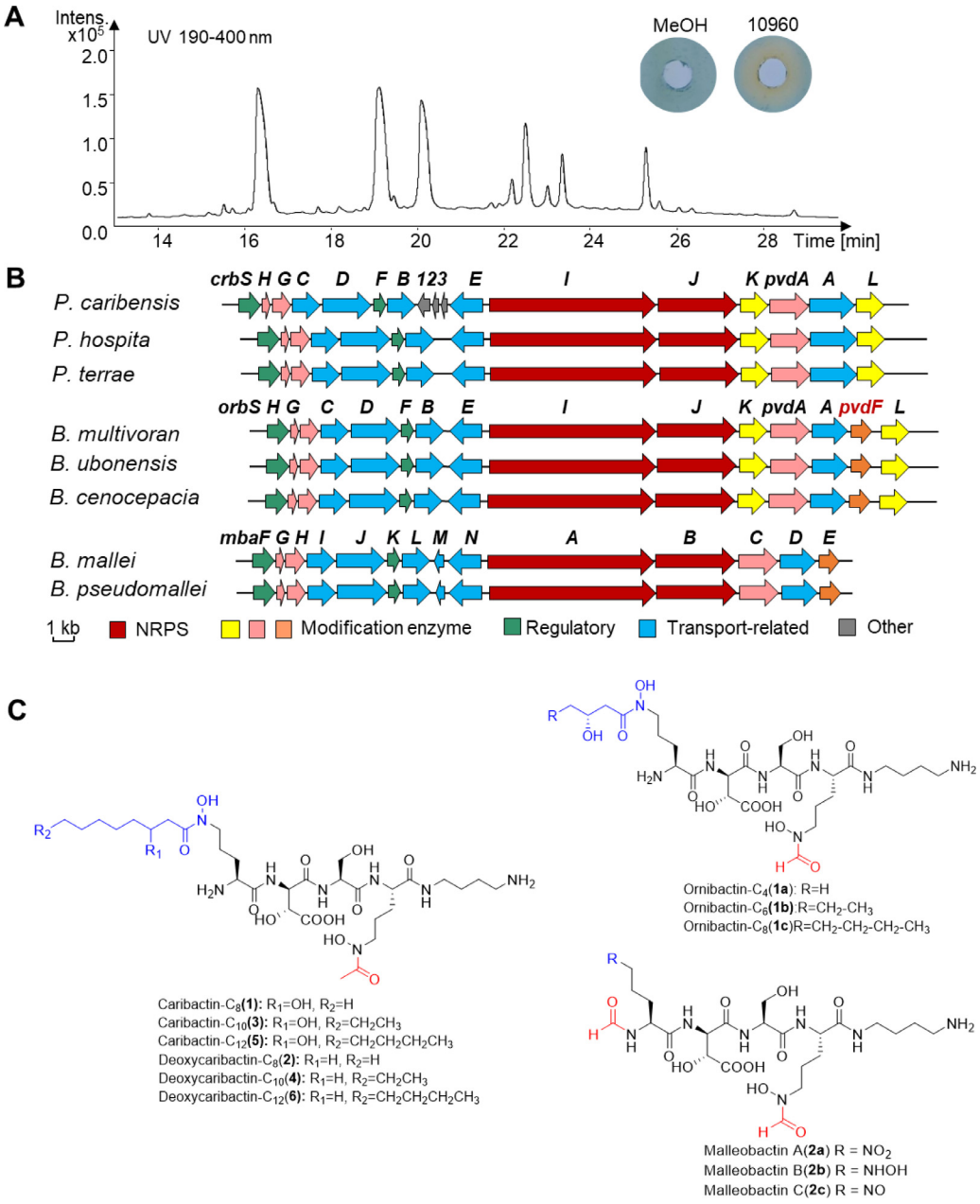

Fig. 1. Siderophore activity and analysis of *crb, orb*, and *mba* biosynthetic gene clusters and their structures. **(A)** CAS agar assay and HPLC-MS analysis of the siderophores cultivated by the CICC 10960 strain when stirred in iron-deficient medium. **(B)** Comparison of caribactin, malleobactin, and ornibactin biosynthetic gene clusters (*crb, orb*, and *mba*, respectively). **(C)** Structures of the caribactins, ornibactins, and malleobactins.

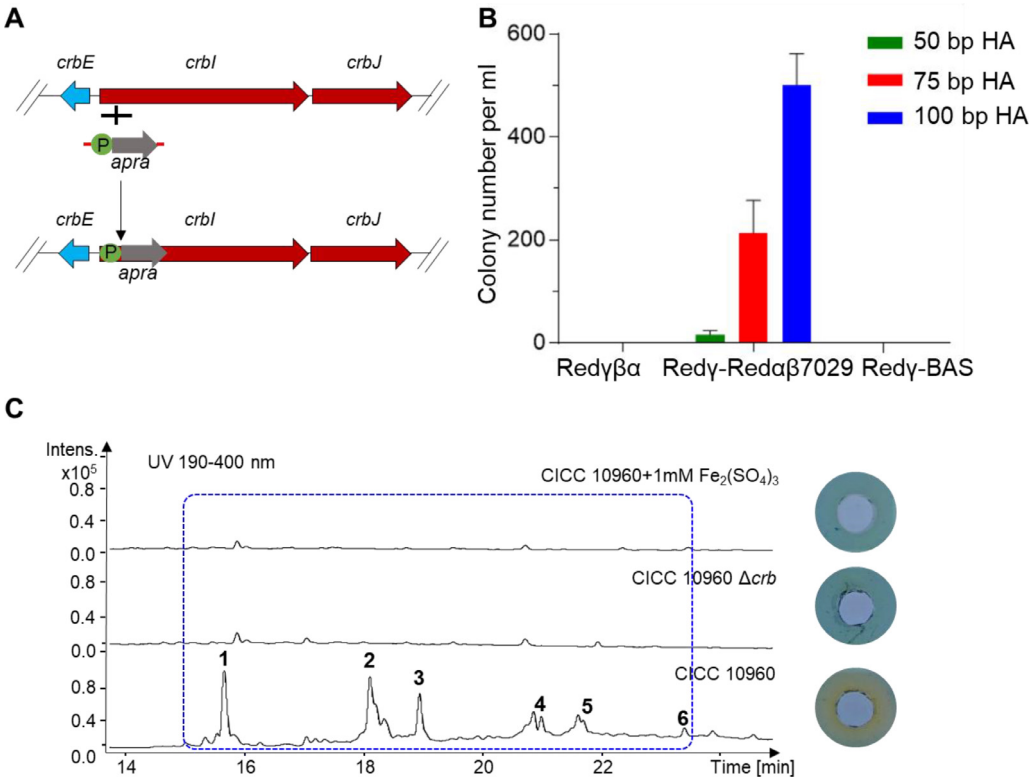

Fig. 2. Establishment of recombineering system in stain CICC 10960 to verify the production of *crb* BGC. **(A)** Diagram of knockout of *crb* gene cluster in strain CICC 10960. **(B)** Recombination efficiency comparison of three recombinases: Red$\gamma\beta\alpha$, Redγ-Red$\alpha\beta$7029, and Redγ-BAS. **(C)** CAS agar assay and HPLC-MS analysis of the siderophore cultivated by the CICC 10960 strain when stirred in iron-deficient and iron-rich medium, and CICC 10960 Δ*crb* strain stirred in iron-deficient medium.

and CrbJ (C_4-A_4-T_4, C_5) to form the tetrapeptidyl backbone; however, their accessory genes differ (Fig. 1B). The *crb* BGC does not have the formyltransferase-encoding gene *pvdF*, which is present in *orb* and *mba* BGCs. The *mba* BGC does not have the two acyltransferase-encoding genes *orbK* and *orbL*, which are present in *crb* and *mba* BGCs.

Genes *pvdA, orbL*, and *pvdF* in *orb* BGC are responsible for ornithine hydroxylation, fatty acid chain loading, and formylation processes, respectively [34–36], to biosynthesize the key amino acid residue N-δ-hydroxy-N-δ-formylornithine (hfOrn) (Table S7). The absence of *pvdF* in *crb* BGCs (Fig. 1C) suggests that *P. caribensis* CICC 10960 produces novel siderophores different to ornibactin and malleobactin.

The *crb* BGCs are generally distributed in the genomes of the genus *Paraburkholderia* including the environmental species *P. caribensis, P. hospital*, and *P. terrae* [37]. The *orb* and *mba* BGCs [38–42] are mostly present in the genus *Burkholderia* containing pathogenic organisms [43] (Fig. 1B). This phenomenon shows the possible evolutionary correlation of these siderophore biosynthetic pathways, suggesting that the two genera of *Burkholderiales* have different siderophores may because of their presence in different environments.

3.2. Establishment of recombineering system to identify caribactin

To verify the production of *crb* BGC, we attempted to establish feasible gene manipulation tools in strain CICC 10960 by screening three recombination systems: Red$\gamma\beta\alpha$ from *Escherichia coli*, Redγ-Red$\alpha\beta$7029, and Redγ-BAS [20–22]. Each recombinase pair was introduced separately into strain CICC 10960 via electrotransformation to assess its feasibility. The 1,218 bp fragment (2,228,707–2,229,924) of the *crbI* gene was replaced with an apramycin resistance gene flanked by homology arms of different lengths (50 bp, 75 bp, 100 bp) (Fig. 2A). The correct recombinant proteins were confirmed using colony PCR. Redγ-Red$\alpha\beta$7029 was highly efficient in genome modification with all three homology arm lengths and thus was selected for further genome manipulation in strain CICC 10960. By contrast, Red$\gamma\beta\alpha$ and Redγ-BAS were not effective in strain CICC 10960 when using 50 bp, 75 bp, and 100 bp homology arms (Fig. 2B). Next, the Redγ-Red$\alpha\beta$7029 system was selected for genome editing in strain CICC 10960. We then investigated whether the siderophore-encoding BGC in CICC 10960 was active by culturing the strain in an iron-deficient (M9 medium) or iron-rich (M9 + 1 mM $Fe_2(SO_4)_3$) medium. The Δ*crb* mutant showed same peak pattern as observed in an iron-rich environment (Fig. 2C). These results confirmed that *crb* BGC was responsible for the biosynthesis of the siderophore (caribactin). Overall, our findings demonstrate the feasibility of using the Redγ-Red$\alpha\beta$7029 recombineering system for genetic manipulation in strain CICC 10960 and the essential role of *crb* BGC in siderophore biosynthesis.

3.3. Isolation and structure determination of caribactins

The compounds were purified from an 8.5 L fermentation culture. Compounds **1–6** (Figs. 2C and S2) were isolated, and their structures were determined using extensive NMR analysis, HRESIMS data, and Marfey's method. Caribactin-C_8 (**1**) was obtained as a white powder with the molecular formula $C_{31}H_{58}N_8O_{13}$ based on the HRESIMS peaks at *m/z* 751.4199 $[M + H]^+$. The ^{13}C NMR spectrum of **1** showed a duplicate carbon signal (Table S1). Analysis of the ^1H, ^{13}C, DEPT, and HSQC NMR spectra of **1** revealed signals for five amide groups (δ_C 171.5, 169.1, 168.5, 169.9, 171.3), one amidated methylene ($\delta_{H/C}$ 2.77/38.5) pertaining to putrescine, one acetyl carbon (δ_C 170.6 and $\delta_{H/C}$ 2.0/20.3), four α-methines of amino acid derivatives ($\delta_{H/C}$ 3.97 /52.0, 4.82/55.4, 4.38/54.9, 4.18/52.8), an oxygenated methylene ($\delta_{H/C}$ 3.51, 3.64/61.8) belonging to serine, an oxygenated methine ($\delta_{H/C}$ 4.51/70.5), and a carboxyl carbon (δ_C 172.8) belonging to β-OH-Asp. These characteristic signals are similar to those reported in the literature

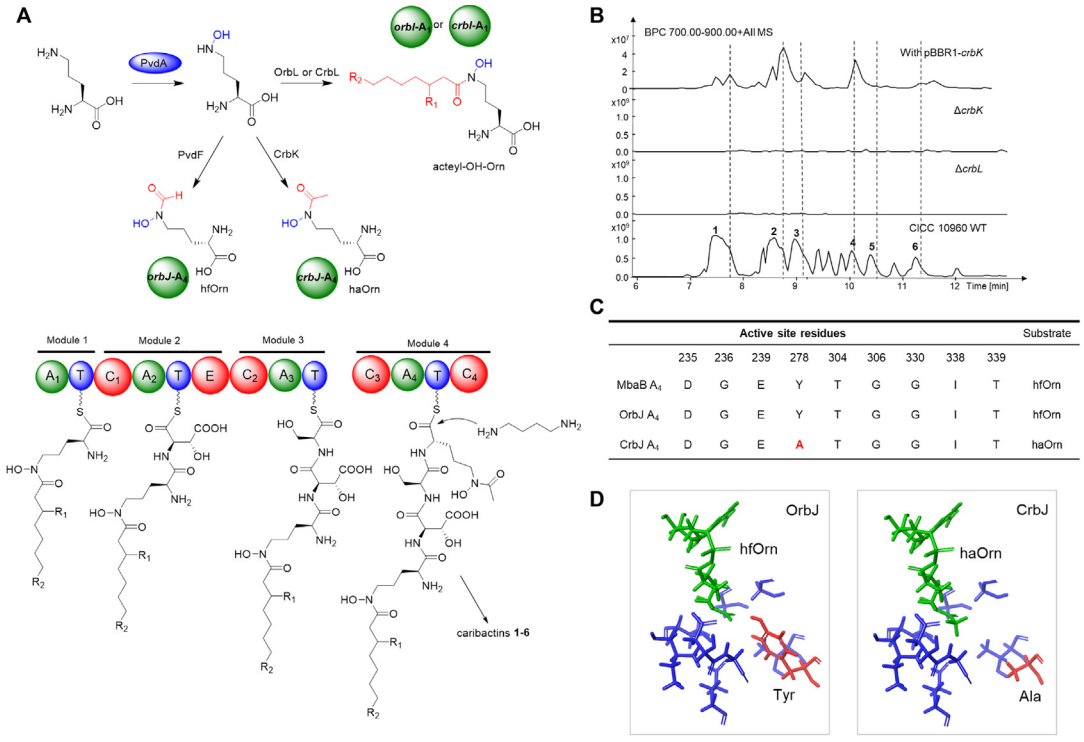

Fig. 3. Proposed biosynthetic pathway for caribactins and to verify *crbK* gene function. **(A)** Proposed biosynthetic pathway for caribactins. **(B)** Analysis of *crb* BGC through LC–MS analysis of the metabolic profiles of wild type, Δ*crbK* mutant, pBBR1-*crbK* in Δ*crbK* mutant, and Δ*crbL* mutant. **(C)** Alignment core motifs A_4 putatively activating hfOrn (MbaB-A_4, OrbJ-A_4) and haOrn (CrbJ-A_4). **(D)** Molecular docking interaction of hfOrn with OrbJ-A_4 and haOrn2 with CrbJ-A_4.

for ornibactin compounds. An acetyl group (δ_C 170.6 and $\delta_{H/C}$ 2.0/20.3) was identified as part of N-δ-hydroxy-N-δ-acetylornithine (haOrn) in **1**, which differed from the hfOrn in ornibactin structure. In addition, an oxygenated methine signal, five methylene signals, and one methyl group were identified as 3-OH caprylic acid connected to N-δ-hydroxy-ornithine (hOrn) by an amide bond, according to the ^{13}C, ^{1}H, COSY, and HMBC NMR spectra (Fig. S2). The amino acid configurations of **1** were determined using reductive hydrolysis followed by derivatization with Nα-(2,4-dinitro-5-fluorophenyl)-L-alaninamide (L-FDLA) and HPLC-MS analysis, which showed that Orn, β-OH-Asp, and Ser in **1** were L-Orn, *threo*-β-OH-D-Asp, and L-Ser, respectively (Fig. S1).

Deoxycaribactin-C_8 (**2**) was isolated as a white powder, indicated by the HRESIMS signal at *m/z* 734.4174 $[M + H]^+$, which was 16 Da smaller than that of **1**. Analysis of the 1D NMR data of **2** revealed the presence of the same core group as **1** (Table S2). Although **1** and **2** had closely related NMR data, the oxygenated methine signal ($\delta_{H/C}$ 3.83/66.8) changed to methylene ($\delta_{H/C}$ 1.58/21.88) in the acyl side chain of **2**, indicating that the acyl group was caprylic acid instead of 3-OH caprylic acid.

Similarly, Caribactin-C_{10} (**3**) was obtained as a white powder and was determined from the HRESIMS signal at *m/z* 778.4436 $[M + H]^+$, with a molecular formula of $C_{33}H_{62}N_8O_{13}$, suggesting two more CH_2 groups than in **1** (Table S3). Two additional methylene signals were identified as part of the acyl group and constituted 3-OH-decylic acid in **3** via NMR analysis. The structures of deoxycaribactin-C_{10}, caribactin-C_{12}, and deoxycaribactin-C_{12} (**4–6**) were deduced using comparative HRESIMS/MS fragment analysis (Supplementary Figs. 2–4).

3.4. Biosynthetic pathway of siderophore caribactins

Caribactins are composed of L-haOrn-D-Asp-L-Ser-L-haOrn. The structural disparity between caribactins and ornibactins can be attributed to the absence of homologs of *pvdF*, a gene encoding a formyltransferase, in the *crb* gene cluster. The biosynthetic pathway of ornibactins involves the loading of acyl chains to the first N-δ-hydroxy-ornithine (hOrn1) by the *orbL* gene, and the function of *orbK* has not been described in the literature [35]. Therefore, we inferred that *crbK* may be responsible for the second N-δ-hydroxy-ornithine (hOrn2) (Fig. 3A). To understand the roles of *crbK* and *crbL* in the biosynthesis of caribactins, we used *apra* and *genta* to replace *crbK* and *crbL*, respectively. HPLC-MS analysis showed the absence of six distinct peaks and precursor compounds in the Δ*crbK* and Δ*crbL* mutant strains (Fig. 3B). Furthermore, the expression vector pBBR1-*crbK* containing *crbK* gene was transfected into CICC 10960 Δ*crbK* cells as the complementary experiment. Six peaks were detected for the *crbK* complementary strain CICC 10960 Δ*crbK*/pBBR1-*crbK*. HPLC-MS analysis of these mutants revealed the essential roles of *crbK* and *crbL* in the biosynthesis of caribactins.

Furthermore, we compared the 10 conserved "Stachelhaus code" sites in the adenylation (A) domains MbaB-A_4 (*B. mallei, B. pseudomallei*) and OrbJ-A_4 (*B. multivoran, B. ubonensis, B. cenocepacia*) with CrbJ-A_4 (*P. caribensis, P. hospital, P. terrae*) [31,44] and revealed a change in the 278th amino acid from Y (MbaB-A_4/OrbJ-A_4) to A (CrbJ-A_4) (Fig. 3C). This change resulted in an alteration of the active pocket, which may account for the ability of CrbJ-A_4 to locate a larger haOrn with a short side chain in A278. We used Maestro software to simulate the docking of the OrbJ-A_4/CrbJ-A_4 domain with the corresponding substrates. The results revealed that the Y278 at the active site was too close to the acetyl group of the substrate when the structure of the substrate changed from hfOrn to haOrn (Fig. 3D). A278 on CrbJ-A_4 fits well with the absence of *the pvdF* gene for the loading and incorporation of a haOrn residue in caribactin. OrbJ-A_4 can only load the smaller substrate, hfOrn, but cannot load the bigger substrate, haOrn, even though the haOrn was generated by OrbK, into the NRPS to produce ornibactins owing to the hindrance caused by Y278; this may be the reason why *orbK* is not involved in the previous study of ornibactin biosynthesis [35]. Based on the results of our experiments, we propose that the *crbL* gene may be responsible for connecting the acyl fatty acid chain to the starting N-

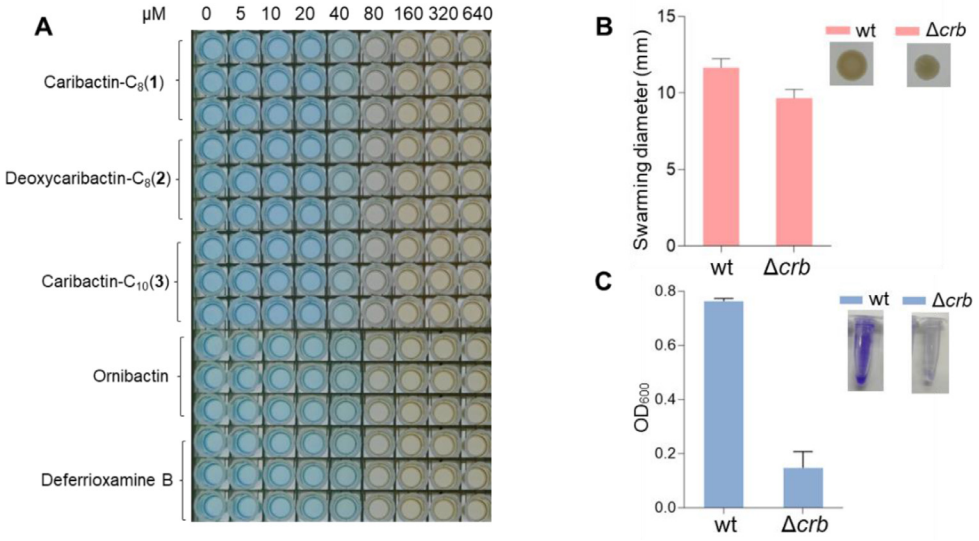

Fig. 4. Bioactivities of caribactins **(A)** Concentration-dependent chrome azurol S (CAS) assay. **(B)** Swarming and swimming assays of wild-type and Δ*crb* mutants. **(C)** Biofilms of wild-type and Δ*crb* mutants measured by the absorbance of OD_{600} nm by using a microplate reader.

δ-hydroxy-ornithine (hOrn1), as shown in ornibactin biosynthesis, and the *crbK* gene may be responsible for the acetylation of the second N-δ-hydroxy-ornithine (hOrn2). These findings suggest a possible biosynthetic pathway for caribactins (Fig. 3A).

3.5. Bioactivities of caribactin

We compared the iron-binding properties of compounds **1, 2**, and **3** with those of ornibactin and the classical siderophore desferrioxamine B using CAS assays (Fig. 4A). These compounds were found to bind to iron and were blue to orange in color, indicating that haOrn slightly affects siderophore activity. These compounds may help bacteria resist the host immune system and gain parasitic advantages through biofilm formation [45]. We measured biofilm formation and swarming motility of the wild-type *P. caribensis* CICC 10960 and the *P. caribensis* CICC 10960 Δ*crb* mutant strain. Caribactin significantly promoted biofilm formation, swarming, and swimming motility of the bacteria (Fig. 4B, C). Siderophores may contribute to the production of biofilms, which can enhance the ability of bacteria to parasitize the host and exert virulent effects [45].

4. Conclusion

We successfully established an efficient genetic manipulation system for *P. caribensis* CICC 10960 that enabled us to verify the products of *crb* BGC via gene knockout experiments. Caribactins and ornibactins share comparable structures but belong to different genera of the *Burkholderiales*. We herein clarified the biosynthetic mechansim for production of different siderophores in two genera, which suggested that the caribactin and oribactin BGCs may have some evolutionary correlation. Based on the gene knockout and complement expression of *crbK*, we proposed that *crbK* gene may be responsible for the acetylation of the second N-δ-hydroxy-ornithine (hOrn2). The results of the alignment of core motifs of the OrbJ-A_4/CrbJ-A_4/MbaJ-A_4 domain and molecular docking of the OrbJ-A_4/CrbJ-A_4 domain with the corresponding substrates demonstrated that position Y278 is essential for substrate selection. Our findings suggested that siderophores promote biofilm production, indicating that siderophores not only regulate bacterial iron balance but also play a crucial role in other regulatory pathways. Hence, siderophores are essential for the physiological activities of bacteria. Moreover, this study showed that recombineering accelerates genome mining of novel secondary metabolites in non-model *Burkholderiales* strains.

Data Availability Statement

All data generated or analyzed during this study are included in this published article and its supplementary information files or are available upon request.

Authorship Contribution Statement

X.Bian conceived the study and supervised the experiments; X.W., H.Z., H.C., L.Z., X.Bai., X.R. and X.Bian designed and conducted construction of mutants and plasmids, fermentation, metabolic analyses purification of compounds and bioactivity assays, H.Z. performed structural elucidation, X.W., H.Z., H.C., L.Z., X.Bai, X.R., and X.Bian analyzed the experimental data, X.W., H.Z. and X.Bian wrote the paper with the input from all authors.

Declaration of Competing Interest

The authors declare that they have no known competing financial interests or personal relationships that could have appeared to influence the work reported in this paper

Acknowledgement

We thank Haiyan Sui, Zhifeng Li, Jingyao Qu, Guannan Lin, and Jing Zhu from the State Key Laboratory of Microbial Technology of Shandong University for their assistance with NMR and LC–HRMS. This work was supported by the National Key R&D Program of China (2019YFA0905700) and National Natural Science Foundation of China (32070060).

Supplementary materials

Supplementary material associated with this article can be found, in the online version, at doi:10.1016/j.engmic.2023.100106.

References

[1] J.E. Cassat, E.P. Skaar, Iron in infection and immunity, Cell Host Microbe 13 (5) (2013) 509–519.
[2] P.T. Lieu, M. Heiskala, P.A. Peterson, et al., The roles of iron in health and disease, Mol. Aspects Med. 22 (1–2) (2001) 1–87.
[3] S.W. Stites, M.W. Plautz, K. Bailey, et al., Increased concentrations of iron and isoferritins in the lower respiratory tract of patients with stable cystic fibrosis, Am. J. Respir. Crit. Care Med. 160 (3) (1999) 796–801.

[4] G. Swayambhu, M. Bruno, A.M. Gulick, et al., Siderophore natural products as pharmaceutical agents, Curr. Opin. Biotechnol. 69 (2021) 242–251.
[5] A. Mathew, C. Jenul, A.L. Carlier, et al., The role of siderophores in metal homeostasis of members of the genus *Burkholderia*, Environ. Microbiol. Rep. 8 (1) (2016) 103–109.
[6] P.J. Keeling, Functional and ecological impacts of horizontal gene transfer in eukaryotes, Curr. Opin. Genet. Dev. 19 (6) (2009) 613–619.
[7] E. Mahenthiralingam, A. Baldwin, C.G. Dowson, et al., *Burkholderia cepacia* complex bacteria: opportunistic pathogens with important natural biology, J. Appl. Microbiol. 104 (6) (2008) 1539–1551.
[8] Q. Esmaeel, M. Pupin, N.P. Kieu, et al., *Burkholderia* genome mining for nonribosomal peptide synthetases reveals a great potential for novel siderophores and lipopeptides synthesis, MicrobiologyOpen 5 (3) (2016) 512–526.
[9] Q. Esmaeel, M. Pupin, P. Jacques, et al., Nonribosomal peptides and polyketides of *Burkholderia*: new compounds potentially implicated in biocontrol and pharmaceuticals, Environ. Sci. Pollut. Res. Int., 25 (30) (2018) 29794–29807.
[10] S. Kunakom, A.S. Eustaquio, *Burkholderia* as a source of natural products, J. Nat. Prod. 82 (7) (2019) 2018–2037.
[11] E. Depoorter, E.D. Canck, T. Coenye, et al., *Burkholderia* bacteria produce multiple potentially novel molecules that inhibit carbapenem-resistant gram-negative bacterial pathogens, Antibiotics (Basel) 10 (2) (2021) 147.
[12] G.J. Jeong, F. Khan, S. Khan, et al., *Pseudomonas aeruginosa* virulence attenuation by inhibiting siderophore functions, Appl. Microbiol. Biotechnol. 107 (4) (2023) 1019–1038.
[13] M.S. Thomas, Iron acquisition mechanisms of the *Burkholderia cepacia* complex, Biometals 20 (3–4) (2007) 431–452.
[14] J. Masschelein, M. Jenner, G.L. Challis, Antibiotics from Gram-negative bacteria: a comprehensive overview and selected biosynthetic highlights, Nat. Prod. Rep. 34 (7) (2017) 712–783.
[15] S.P. Niehs, B. Dose, K. Scherlach, et al., Genome mining reveals endopyrroles from a nonribosomal peptide assembly line triggered in fungal-bacterial symbiosis, ACS Chem. Biol. 14 (8) (2019) 1811–1818.
[16] X. Liu, Y.Q. Cheng, Genome-guided discovery of diverse natural products from *Burkholderia* sp, J. Ind. Microb. Biotechnol. 41 (2) (2014) 275–284.
[17] L. Li, Next-generation synthetic biology approaches for the accelerated discovery of microbial natural products, Eng. Microbiol. 3 (1) (2023) 100060.
[18] A.R. Barrett, Y. Kang, K.S. Inamasu, et al., Genetic tools for allelic replacement in *Burkholderia* species, Appl. Environ. Microb. 74 (14) (2008) 4498–4508.
[19] Y. Kang, M.H. Norris, B.A. Wilcox, et al., Knockout and pullout recombineering for naturally transformable *Burkholderia thailandensis* and *Burkholderia pseudomallei*, Nat. Protoc. 6 (8) (2011) 1085–1104.
[20] X. Wang, H. Zhou, H. Chen, et al., Discovery of recombinases enables genome mining of cryptic biosynthetic gene clusters in *Burkholderiales* species, Proc. Natl. Acad. Sci. USA. 115 (18) (2018) E4255–E4263.
[21] J. Yin, W. Zheng, Y. Gao, et al., Single-stranded DNA-binding protein and exogenous RecBCD inhibitors enhance phage-derived homologous recombination in *Pseudomonas*, iScience 14 (2019) 1–14.
[22] J. Fu, X. Bian, S. Hu, et al., Full-length RecE enhances linear-linear homologous recombination and facilitates direct cloning for bioprospecting, Nat. Biotechnol. 30 (5) (2012) 440–446.
[23] R. Li, H. Shi, X. Zhao, et al., Development and application of an efficient recombineering system for *Burkholderia glumae* and *Burkholderia plantarii*, Microb. Biotechnol. 14 (4) (2021) 1809–1826.
[24] H. Chen, L. Zhong, H. Zhou, et al., Biosynthesis of glidomides and elucidation of different mechanisms for formation of beta-OH amino acid building blocks, Angew. Chem. Int. Ed. 61 (35) (2022) e202203591.
[25] H. Chen, T. Sun, X. Bai, et al., Genomics-driven activation of silent biosynthetic gene clusters in *Burkholderia gladioli* by screening recombineering system, Molecules 26 (3) (2021) 700.
[26] W. Zheng, X. Wang, H. Zhou, et al., Establishment of recombineering genome editing system in *Paraburkholderia megapolitana* empowers activation of silent biosynthetic gene clusters, Microb. Biotechnol. 13 (2) (2020) 397–405.
[27] H. Chen, H. Zhou, T. Sun, et al., Identification of holrhizins E-Q reveals the diversity of nonribosomal lipopeptides in *Paraburkholderia rhizoxinica*, J. Nat. Prod. 83 (2) (2020) 537–541.
[28] S. Kodani, H. Komaki, M. Suzuki, et al., Structure determination of a siderophore peucechelin from *Streptomyces peucetius*, Biometals 28 (5) (2015) 791–801.
[29] F. Zhang, K. Barns, F.M. Hoffmann, et al., Thalassosamide, a siderophore discovered from the marine-derived bacterium *Thalassospira profundimaris*, J. Nat. Prod. 80 (9) (2017) 2551–2555.
[30] T. Thongkongkaew, W. Ding, E. Bratovanov, et al., Two types of threonine-tagged lipopeptides synergize in host colonization by pathogenic *Burkholderia* species, ACS Chem. Biol. 13 (5) (2018) 1370–1379.
[31] C. Lee, M. Mannaa, N. Kim, et al., Stress tolerance and virulence-related roles of lipopolysaccharide in *Burkholderia glumae*, Plant Pathol. J. 35 (5) (2019) 445–458.
[32] K. Blin, S. Shaw, H.E. Augustijn, et al., antiSMASH 7.0: new and improved predictions for detection, regulation, chemical structures and visualisation, Nucleic. Acids. Res. (2023) gkad344.
[33] H. Stephan, S. Freund, W. Beck, et al., Ornibactins–a new family of siderophores from *Pseudomonas*, Biometals 6 (2) (1993) 93–100.
[34] P.A. Sokol, P. Darling, D.E. Woods, et al., Role of ornibactin biosynthesis in the virulence of *Burkholderia cepacia*: characterization of *pvdA*, the gene encoding L-Ornithine N^5-oxygenase, Infect. Immun. 67 (9) (1999) 4443–4455.
[35] J. Franke, K. Ishida, C. Hertweck, Evolution of siderophore pathways in human pathogenic bacteria, J. Am. Chem. Soc. 136 (15) (2014) 5599–5602.
[36] P. Philem, T. Kleffmann, S. Gai, et al., Identification of active site residues of the siderophore synthesis enzyme PvdF and evidence for interaction of PvdF with a substrate-providing enzyme, Int. J. Mol. Sci. 22 (4) (2021) 2211.
[37] A.A. Pratama, D.J. Jiménez, Q. Chen, et al., Delineation of a subgroup of the genus *Paraburkholderia*, including *P. terrae* DSM 17804T, *P. hospita* DSM 17164T, and four soil-isolated fungiphiles, reveals remarkable genomic and ecological features-proposal for the definition of a *P. hospita* species cluster, Genome Biol. Evol. 12 (4) (2020) 325–344.
[38] C. Peeters, V.S. Cooper, P.J. Hatcher, et al., Comparative genomics of *Burkholderia multivorans*, a ubiquitous pathogen with a highly conserved genomic structure, PLoS One 12 (4) (2017) e0176191.
[39] E.P. Price, D.S. Sarovich, J.R. Webb, et al., Phylogeographic, genomic, and meropenem susceptibility analysis of *Burkholderia ubonensis*, PLoS Negl. Trop. Dis. 11 (9) (2017) e0005928.
[40] A. Wallner, E. King, E.L.M. Ngonkeu, et al., Genomic analyses of *Burkholderia cenocepacia* reveal multiple species with differential host-adaptation to plants and humans, BMC Genom. 20 (1) (2019) 803.
[41] S.L. Johnson, K.A. Bishop-Lilly, J.T. Ladner, et al., Complete genome sequences for 59 *Burkholderia* isolates, both pathogenic and near neighbor, Genome Announc. 3 (2) (2015) e00159-15.
[42] E.P. Price, D.S. Sarovich, L. Viberg, et al., Whole-genome sequencing of *Burkholderia pseudomallei* isolates from an unusual melioidosis case identifies a polyclonal infection with the same multilocus sequence type, J. Clin. Microbiol. 53 (1) (2015) 282–286.
[43] A. Sawana, M. Adeolu, R.S. Gupta, Molecular signatures and phylogenomic analysis of the genus *Burkholderia*: proposal for division of this genus into the emended genus *Burkholderia* containing pathogenic organisms and a new genus *Paraburkholderia* gen. nov. harboring environmental species, Front. Genet. 5 (2014) 429.
[44] T. Stachelhaus, H.D. Mootz, M.A. Marahiel, The specificity-conferring code of adenylation domains in nonribosomal peptide synthetases, Chem. Biol. 6 (8) (1999) 493–505.
[45] K. Pokharel, B.R. Dawadi, L.B. Shrestha, Role of biofilm in bacterial infection and antimicrobial resistance, JNMA J. Nepal Med. Assoc. 60 (253) (2022) 836–840.